Test for Covid-19 seasonality and the risk of second waves

Francois A. Engelbrecht (Francois.Engelbrecht@wits.ac.za)
University of the Witwatersrand
Robert J. Scholes
University of the Witwatersrand

Research Article

Keywords: Covid-19 seasonality, second waves, SIRD model, test

Posted Date: August 2nd, 2020

DOI: https://doi.org/10.21203/rs.3.rs-50313/v1

Version of Record: A version of this preprint was published at One Health on June 1st, 2021. See the published version at https://doi.org/10.1016/j.onehlt.2020.100202.

Abstract

Eight months into the Covid-19 pandemic it remains unclear whether transmission of SARS-CoV-2 is affected by climate factors. Using a dynamic epidemiological model with Covid-19 climate sensitivity in the likely range, we demonstrate why attempts to detect a climate signal in Covid-19 have thus far been inconclusive. Then we formulate a novel methodology and related criteria that can be used to test for seasonal climate sensitivity in observed Covid-19 infection data. We show that if the disease *does* have a substantial seasonal dependence, and herd immunity is not established during the first peak season of the outbreak (or a vaccine does not become available), there is likely to be a seasonality-sensitive second wave of infections about one year after the initial outbreak. In regions where non-pharmaceutical control has contained the disease in the first year of outbreak and thus kept a large portion of the population susceptible, the second wave may be substantially larger in amplitude than the first if control measures are relaxed. This is simply because it develops under the favorable conditions of a full autumn to winter period and from a larger pool of infected individuals.

1. Introduction

Three of the four commonly circulating human coronaviruses exhibit pronounced seasonality in terms of when infection rates peak every year (e.g. Gaunt et al., 2010; Baker et al., 2020; Neher et al., 2020; Nickbakhsh et al., 2020). Influenza is a related viral infection, and although not caused by a coronavirus, the “influenza season” is a well-established phenomenon in mid-latitude countries (Shaman et al., 2010; Petrova et al., 2020). The seasonal dependence of viral respiratory diseases has been attributed to several potential mechanisms, including among others the viruses being less stable and less transmissible in air at higher temperatures (e.g. Lowen et al., 2008), virus-carrying droplets falling out of the air relatively faster in humid air (e.g. Lowen et al., 2007); the sensitivity of the virus to UV radiation (e.g. Sagripanti and Lytle, 2007), increased viral susceptibility of the human victim in cold and dry weather (e.g. Shaw Stewart, 2016; Kudo et al., 2019) and changes in human social behavior between winter and summer (e.g. Lofgren et al., 2007).

The initial Covid-19 outbreak in December 2019 occurred in mid-latitude Northern Hemisphere countries during the boreal winter. The disease reached Summer Hemisphere countries from about February 2020, during the austral late summer to early autumn. It is of considerable practical interest to understand whether Covid-19 has a strong seasonality dependence. For instance, will its spread be enhanced in mid latitude Southern Hemisphere countries during the winter of 2020, and will infection rates simultaneously be reduced by warm and humid weather during the Northern Hemisphere summer? Disentangling the effects of climate seasonality, if it exists, from the effects of the extremely variable non-pharmaceutical interventions (e.g. regulated lockdown and self-imposed social distancing) is necessary to understand the potential future behavior of the disease, particularly in the second year of infection, when the Northern Hemisphere returns to winter in late 2020, followed by the Southern Hemisphere six months later. A seasonal effect is potentially an important contributor to the occurrence of a second wave of outbreaks. Moreover, will Covid-19 become an annual occurrence, like many viral respiratory diseases?

Several studies to date have attempted to identify and quantify climatic dependencies in Covid- 19 infection rates, using data on reported cases (e.g. Ficetola and Rubolini, 2020; Merow and Urban, 2020; Qi et al., 2020; Sajadi et al., 2020), but have failed to conclusively prove or disprove the existence of such a link. These studies have been compromised by the fact that no single location on Earth has yet moved through a full annual cycle in the presence of Covid-19; thus the studies depend on 'space-for-time' substitution (in other words, using the difference in climate between different locations as a proxy for its evolution over time in one location) – but the assumptions necessary for this approach to work are confounded by the spatial dynamic of the disease spread. Moreover, various degrees of non-pharmaceutical control measures have been applied across different countries, and their intensity changes over time at a given location. This, in combination with differential socio-economic conditions and related differential abilities of individuals to apply social distancing, makes it hard to identify a relatively weak climatic signal in observed case data. Further noise is added by the heterogeneity in how the case data and mortality data are reported. The initial scarcity of definitive tests resulted in a biased sampling of case load, since testing was largely confined to people who reported symptoms, and those who had been in contact with them. Vast discrepancies in testing rate and testing strategy still persist between countries. Finally, Baker et al. (2020) used a dynamic epidemiological model to argue that when the number of susceptible individuals in a population is high, as occurs in the initial stages of a novel disease, the subtle effects of seasonality are swamped by the high basic disease reproduction rate. As a consequence of all these complicating factors, by July 2020, no consensus has been reached on whether Covid-19 has a climatic dependence; and if so, which environmental factors are involved, and what their relative strength is (e.g. O'Reilly et al., 2020).

Here we make use of a dynamic epidemiological model to identify the 'signature' of seasonality in the outbreak of a highly infectious disease such as Covid-19. This allows us to propose how this signature may be detected in observed case data. We then analyse the conditions under which Covid-19 may resurge as a second wave of infections, and how this relates to seasonality.

2. Methods

Idealised profiles of seasonality provides a standard approach in modelling infectious diseases with seasonal behaviour (e.g. Dushoff et al., 2004; Chen and Epureanu, 2017; Neher et al., 2020). Following this approach, we define a 'Theoretical Climate Correction Factor' (TCCF) that describes how seasonality may modify the basic reproductive number R_0:

$$TCCF = \left(\frac{1}{1+\varepsilon}\right)\left(1 + \varepsilon\cos\left(2\pi(t-\theta)\right)\right). \quad (1)$$

Here ε ranges from 0 to 1 and represents the strength of seasonality, with transmissibility reaching a peak when = θ . That is, in this paper the basic reproductive number R0 is the expected number of secondary infectious cases generated by an average infectious case in an entirely susceptible population

under climatological conditions optimal for transmission (when $t = \theta$). Consistently, $0 \leq \left(\frac{1-\epsilon}{1+\epsilon}\right) \leq TCCF \leq 1$ and $0 \leq R_t \leq R_0$, where R_t is the effective reproduction number ($R_t = TCCF * R_0$).

The TCCF can be explored over the full ranges of amplitude and timing, but we are also interested in the more limited expression of seasonality that we actually observe in the world. For this we define a simple empirical function, the 'Climate Correction Factor', CCF. We base the CCF function on data from China (Wang et al., 2020), noting qualitatively similar findings from other studies in China, Europe and North America (Ficetola and Rubolini, 2020; Qi et al., 2020; Sajadi et al., 2020). These studies have suggest that the basic reproduction rate has a broad maximum when the daily mean temperature Tm is less than 11° C (there is some suggestion of lower rates in extremely cold conditions, but the data are sparse), and then declines at higher temperatures at a rate of about 2.3% per °C. To this function we add an additional condition through which humidity further decreases the infection rate at absolute humidities above 9 g $H2O\ m^{-3}$ (Bukhari and Jameel, 2020):

$$\begin{aligned} &\text{If } T_m < 11 \text{ then } CCF = 1 \\ &\text{else } CCF = 1 - (T_m - 11) * 0.023 \\ &\text{if } H > 9 \text{ then } CCF = 0.9 * CCF \end{aligned} \qquad (2)$$

Like TCCF, the CCF is a dimensionless multiplier of the basic transmission rate, but ranges, based on the climate of actual locations, between about 0.5 and 1. We *do not* claim that it represents a precise or definitive formulation for the climate effect. We use it as the simplest possible representation of the temperature and humidity effects, constrained to the plausible magnitude and form as revealed by the currently available data. We use CCF and TCCF to perform sensitivity tests on how seasonality may influence disease propagation dynamics. In the results section we show how (2) can be interpreted within the theoretical framework provided by (1).

We explore the signatures of seasonality in Covid-19 infection rates using a dynamic epidemiological model forced with seasonality impacts as described by (1) and (2), for the cases of mid-winter and mid-summer outbreak of the disease. In the paper, 'mid-winter' means 1 July (1 January) in the Southern (Northern) Hemisphere, and 'mid-summer' means 1 January (1 July) in the Southern (Northern) Hemisphere. For the case of (1), 'mid-winter' corresponds to the time during which the function attains its maximum value, and mid-summer to the time it reaches a minimum value. Application of (1) makes no assumptions on the underlying causes of seasonality or the time of the year when optimal conditions are reached. The CCF, on the other hand, is driven by climate observations. We use average monthly temperature and absolute humidty climatologies calculated for the period 2009-2018 using the Climatic Research Unit (CRU) TS4.03 data set (Harris and Jones, 2020). The realistic example we chose of warm-dry seasonality is the Gauteng Province in the central interior of South Africa, with Johannesburg as capital. This is a summer rainfall region exhibiting pronounced warm-cold (and moist-dry) continental seasonailty. Daily climatologies of temperature and humidity are needed for a smooth description of seasonality. A simulated climatology from a regional climate model at 0.1° resolution is used for this

purpose (Engelbrecht et al, 2019). The simulated seasonality is bias-corrected to the CRU TS4.03 data following the methodology of Engelbrecht et al. (2015).

The epidemiological model used is a Susceptible-Infectious-Recovered-Dead (SIRD) model with core set of parameters based on the initial outbreak in China, following Anastassopoulou et al (2020):

$$\frac{dS}{dt} = -\frac{\alpha}{N}SI;$$
$$\frac{dI}{dt} = \frac{\alpha}{N}SI - \beta I - \gamma I; \quad (3)$$
$$\frac{dR}{dt} = \beta I;$$
$$\frac{dD}{dt} = \gamma I.$$

Here S, I, R and D are the number of susceptible, infected, recovered and dead individuals, respectively, at a given moment in time, and they sum to the total population, N (which is assumed to remain constant). The core parameter settings are α = 0.319 d^{-1}, γ = 0.0005 d^{-1} and β = 0.16 d^{-1}. Here α is the daily infection rate, γ the mortality rate and β the recovery rate. $R_0 = \frac{\alpha}{\gamma+\beta} \approx 2$ for these settings. In the applications of the SIRD model described in this paper, α is modified to produce various different values of R0, but β and γ are fixed in all the simulations. Seasonality and non-pharmaceutical control measures are both modelled to impact on R0 through changes in α .

The time it takes for an infectious disease to propagate through a population does depend on the size of the population. In the experiments performed here, N = 15 000 000. We further assume that the entire population is susceptible at the time of onset of the disease with the sole focus of exploring seasonality impacts, and not considering the potentially important role of cross-immunity that may exist in populations due to exposure to other coronaviruses (e.g. Sette and Crotty, 2020) or potential cross-protection from for example BCG vaccination programmes (e.g. Escobar et al., 2020). Moreover, we do not distinguish between the symptomatic or asymptomatic infected and it is assumed that members from the population that recover from the disease have immunity for at least two years. The simulations do not take into account any pharmaceutical control measures that may be developed in the future.

3. Results

3.1 Climate correction factor

An example of the spatial application of the CCF as described by (2) is shown for South Africa in Figure 1, for January (summer), April (autumn), July (winter) and October (spring). The CCF reaches its optimal value in winter, whilst mid-summer conditions effectively reduce the infection rate by about 40%. The seasonal cycle in the CCF is shown in Figure 2b for Johannesburg. It may be noted that under (2)

relatively high values of absolute humidity reduce the the infection rate between late spring and early autumn in the interior of continental South Africa.

TCCF seasonal cycles are shown in Figure 2a for a range of values of ε. The fractional increase from the trough to the crest of the wave ('seasonality amplitude') are listed in Table 1 for various values of ε, allowing us to later link generalized TCCF-based analyses to specific CCF analyses.

Table 1: Seasonality strength (ε) and seasonality amplitudes (εA) of the TCCF.

ε (Seasonality strength)	0.1	0.15	0.2	0.25	0.3	0.35	0.4
εA (Seasonality amplitude)	1.22	1.35	1.5	1.67	1.85	2.08	2.33

Two recent epidemiological modelling studies have considered the degree to which seasonality may impact on the annual cycles of commonly circulating human coronaviruses. Using climatic dependent inverse modelling applied to case data of the HCoV-HKU1 and HCoV-OC43 coronaviruses, Figure 1 of Baker et al. (2020) suggests $\varepsilon_A \approx 1.67$ ($\varepsilon \approx 0.25$) for HCoV-HKU1 and $\varepsilon_A \approx 1.25$ ($\varepsilon \approx 0.1$) for HCoV-OC43. For four commonly circulating coronaviruses in Sweden, with seasonality described by an equation equivalent to (1), Neher et al. (2020) concluded that for local spread ε = 0.15 but for strong import of cases $0.3 \leq \varepsilon \leq 0.7$.

These studies provide context to the seasonality amplitude of the CCF (expressed as ε_A, the fractional increase from the month of minimum CCF to the month of maximum CCF) across the globe (Figure 3b). Figure 3 reveals that the largest seasonality amplitudes occur poleward of the tropics, and equatorward of 60° latitude in both hemispheres. Within this latitudinal band it generally holds that $0.15 \leq \varepsilon \leq 0.3$. Values of ε_A indicative of $\varepsilon > 0.3$ are largely confined to the subtropics (~ 30 °N and S) whilst values of $0.1 \leq \varepsilon < 0.15$ occur on the equatorward peripheries of the mentioned latitudinal band. ε_A values are by definition somewhat lower when humidity effects are not explicitly considered (Figure 3a). Within the context provided by Figure 3, and consistent with the inverse modelling based estimates of ε provided by Baker et al. (2020) and Neher et al. (2020), we proceed to apply the SIRD model to explore seasonality impacts in the range $0.1 \leq \varepsilon \leq 0.3$.

3.2 Outbreak in mid-winter

The first case we explore is mid-winter onset of the disease in the presence of seasonality described by ε = 0.2 under (1), representative of most mid-latitude regions that exhibit pronounced warm-cold

seasonality, as revealed by the CCF (Figure 3). The susceptible-infected (SI) orbits (time trajectories the SI phase-plane, shown as proportions of the total population, N) for different values of R_0 for the scenario of 'no control measures and no seasonality effects' are shown in black in Figure 4a, b and c. The orbits commence with effectively an entirely susceptible population ($S = N - 1$, $I = 1$), and then follow a hump-shaped trajectory, returning to the S-axis once herd immunity has been reached. The effect of seasonality, in the absence of control measures, is explored in Figure 4a for several values of R_0 (colored orbits), while the effect of non-pharmaceutical control (e.g. Hale et al., 2020) without seasonality effects, is shown in Figure 4b (colored orbits). For the control scenarios it is assumed that after a period of one month of the disease spreading in the population, a lockdown is enforced which reduces the infection rate by 40% (i.e. 0.6 *R_0). The lockdown is maintained for 9 months, through spring, summer and into autumn, followed by light social distancing (i.e. a 10% reduction, 0.9*R_0). The final scenario considered applies the same non-pharmaceutical control measures whilst seasonality is also having an effect (Figure 4c, colored orbits). The corresponding time-evolution of the fraction of the population of infected (I/N) is shown in Figure 5a to d for selected values of R_0, for the scenarios of no control measures and no seasonality (black lines), no control measures in the presence of seasonality (green lines), lockdown followed by social distancing in the absence of seasonality (yellow lines) and finally, lockdown followed by social distancing, both in the presence of seasonality effects (red lines).

In the initial stages of a mid-winter onset the disease with no control measures being applied, $R_t \approx R_0$ in the presence of low temperatures and humidity ($TCCF \approx 1$; $CCF \approx 1$; Figure 2). As winter progresses to spring, progressively warmer conditions reduce Rt. *The telltale signature of such an effect is that the SI-orbits under seasonality (colored lines in Figure 4a) cross the orbits for the scenario of no control and no seasonality.* This effect can be seen in in Figure 4a, most prominently for the lower values of R0 ($R_0 \leq$ 2.2). At these lower infection rates, the diseases takes relatively long to spread through the population, pushing it into spring and allowing seasonality to lower Rt. For example, for R_0 = 2 in the absence of seasonality the peak infection occurs in spring, 3.5 months into the outbreak (Figure 5d, black line). If seasonal effects are at work, the peak infection is reached about two weeks later - but most importantly, the peak of active cases, which is what determines the load on the health system, is almost halved (Figure 5d, green line). The resulting behavior of the disease, in terms of the total fraction of the population eventually infected, resembles that of an infection with constant R_0 = 1.5 (Figure 4a). By the time that the disease has run its course and herd immunity is reached, less than 60% of the population has been infected, while over 80% of the population is infected if seasonality is not at work. In contrast, if the basic reproduction number is high, for example R_0 = 3, the peak infection in the absence of seasonality occurs less than 2 months after introduction of the first infected individual to the population (Figure 5a, black line). Even if seasonality effects are considered, given that climatological effects are optimal for transmission for the case of mid-winter outbreak, there is not enough time for seasonality to impact the infection rate (Figure 5a, green line). Consequently for high R0, with or without seasonality, more than 90% of the population is eventually infected. For intermediate cases (R_0 = 2.6 and R_0 = 2.4)

seasonality also results in only slightly smaller infection peaks (Figure 4b and c, green lines vs black lines), reducing the final number of people infected by less than 10% (Figure 4a).

Control measures such as periods of enforced lockdown followed by various degrees of social distancing effectively slow the spread of the disease in a population (e.g. Lai et al., 2020; Maier and Brockmann, 2020). Stringent lockdown can reduce R_t to less than 1, causing the epidemic to disappear over time as has been reported to be the case for Wuhan, China (Zhang et al., 2020a, b). For less stringent or effective control, where R_t remains >1, the disease continues to spread in the population at a reduced rate (e.g. Pei et al., 2020). If a consistent level of non- pharmaceutical control is maintained for a sufficiently long period, it should still be possible to discern signatures of seasonality from the SI-orbits. This is explored in Figure 4b and c. Note that the range of both the S- and I-axes have been reduced compared to Figure 4a and that only a subset of orbits are shown to avoid clutter. For the illustrated scenario, a strong lockdown was initiated one month after onset of the disease and maintained for 9 months, where after it was replaced by social distancing. The SI-orbits display two main types of behavior. For values of $R_0 \geq 2.2$, although the infection rate is significantly damped, the disease still spreads through most of the population and peak infection occurs within six months of the outbreak (and within the period of stringent lockdown) (Figure 5 a to c, yellow lines). In these cases 50-75 % of the population become infected before herd immunity is reached (Figure 4b). For example, an infection with R_0 = 2.4 plus stringent control effectively follows an orbit of R_0 = 1.43 (Figure 3b; yellow line in Figure 5c). For lower basic reproduction numbers (R_0 = 2) the dampening of the infection rate by control measures is sufficiently strong that no significant outbreak occurs during the 9 month period of lockdown (see the blue line representing R_0 = 2 in Figure 4b and the yellow line up and until month 10 in Figure 5d). However, since herd immunity is not achieved, the disease continues to linger in the population, and breaks out in the months immediately following the relaxation of lockdown measures (Figure 4b blue orbit, Figure 5d, yellow line beyond month 10). In terms of the SI-orbits, the outbreak can be seen as a sudden increase in Rt and the consequent crossing of the orbits of constant R_0.

The presence of seasonality accompanied by onset of the disease in mid-winter implies further dampening of infection rates during the period of stringent lockdown. For R_0 = 3 the characteristic signature of seasonality, namely the crossing of the orbits of constant R_0 is apparent (compare the purple orbits in Figures 4b and c), but despite the combined dampening effects of lockdown and seasonality the diseases still propagates through the population until herd immunity is reached late in spring (Figure 5a, red line) with about 60% of the population infected during the course of the outbreak (purple orbit, Figure 4c). The remaining cases ($R_0 \leq 2.6$) displayed in Figure 4c reveal an entirely different type of behavior, induced by seasonality. For these lower infection rates the combined dampening effect of lockdown and seasonality is sufficiently strong that the peak infection is substantially reduced (Figures 5b to d) and less than 25% of the population becomes infected during the period of stringent lockdown (Figure 4c). High summer temperatures following the initial onset of the disease further damp the infection rate, but since herd immunity is never reached, once lockdown is replaced by less stringent social distancing, the return of lower temperatures and humidity as the next winter approaches systematically increases the

infection rate. Without renewed lockdown, this results in a second wave outbreak, with a significantly higher of peak infection than experienced in the first year of the disease (red lines in Figure 5a to c). This scenario may well be important for Northern Hemisphere countries, where initial onset of the disease occurred in approximately mid-winter, and where anti-body tests suggest that the portion of the population infected by mid-summer is significantly less than 20% (e.g. Pollán et al., 2020).

Sensitivity to various strengths of seasonality is explored in Figure 6. For the case where the disease propagates freely in the population under weak seasonality (ε = 0.1), the crossing of orbits of constant R_0 by the seasonality orbits can only be clearly observed for $R_0 \geq 2.2$. However, the feature can be observed clearly for lower values of R0 where spring arrives and affects infection rate before the disease can propagate through the population. Figure 6b explores the case of the disease propagating under actual daily climatic forcing for the Gauteng Province of South Africa using CCF rather than TCCF, corresponding to $\varepsilon \approx 0.2$ (see Figure 2b).The SI-orbits in Figure 6b closely resemble those in Figure 4a. Under stronger seasonality, for instance ε = 0.3, seasonality can be clearly observed in the SI-orbits, with the additional feature of second waves developing for $R_0 \leq 2$. In these cases damping of the infection rate is so substantial during spring and summer that the disease propagation is substantially slowed down. However, it continues to linger in the population and second waves of infection develop from autumn to winter of the following year. Under a scenario of lockdown various strengths of seasonality result in the SI-orbits (Figures 6d to f) exhibiting similar qualitative behavior to those in the case shown in Figure 4c. The key message is that strong non-pharmaceutical control substantially slows down the spread of the disease and increases the role of the seasonality. The combined effects of strong seasonal damping of infection rates and non-pharmaceutical control imply that even for relatively high values of R_0 only a small portion of the population becomes infected during the period of lockdown. If the control is relaxed, second waves of infections develop in autumn and winter of the following years. The amplitude of these waves increase as a function of seasonality strength (compare for example, the SI orbits for R_0 = 2.6 in Figures 6d, e and f) and can exceed the first wave in severity.

3.3 Outbreak in mid-summer

The impacts of seasonality as described by (1) for ε = 0.2 are profoundly different for a summer onset compared to mid-winter onset of the disease, under the scenario of no control measures being applied. The SI-orbits for the case of a mid-summer outbreak are shown in Figure 7 a-c under scenarios of non-pharmaceutical control and seasonality effects and the corresponding I/N time-evolutions in Figure 8. The black orbits in Figure 7 and black lines in Figure 8 represent the case of no control measures and no seasonality effects and correspond exactly to the equivalent orbits in Figure 4 and lines in Figure 5. The summer season substantially dampens the infection rate ($TCFF \approx 0.7$) and consequently delays the peak infection by about a month for R_0 = 3 (Figure 8a, green line) and two months for R_0 = 2 (Figure 8d, green line). For $R_0 \leq 2$ the damping is so significant that the outbreak only gains momentum in the following winter, reaching the same peak infection (Figure 8d, green line) and infecting the same portion of the population (Figure 7c) as for the corresponding situation of no control measures and no

seasonality (Figure 8d, black line). For larger values of R0 peak infection occurs before the peak in seasonality forcing is reached in winter. By the time of peak infection (early autumn for R_0 = 3 to late autumn R_0 = 2.4), Rt has increased sufficiently for the orbits of constant R0 to be crossed (see the colored orbits in Figure 7a). The dampening of the peak infection by seasonality is substantial, even for these higher values of R0. For example, for R_0 = 3 the dampening of the peak infection is about 40% (Figure 8a) and 10% less of the population is infected by the time herd immunity is reached (Figure 7a).

We next exploring a scenario of non-pharmaceutical control similar to that described for the mid- winter onset, but with lockdown maintained from the end of month one to the end of month 12. For values of R_0 $\gg$ 2.2 even under a stringent lockdown, the disease still runs its course through the population during the first year of the infection. The same will thus be true for all weaker forms of lockdown and social distancing. Nonetheless, the amplitude of the peak infection is substantially reduced and its timing is delayed (Figure 8a to c, yellow lines). For the case of R_0 = 3, the peak infection is reduced by 60% with respect to the case of no control measures (Figure 8a), nevertheless about 70% of the population has been infected by the disease by the time that herd immunity is reached (Figure 7b). The lockdown orbits correspond to cases of constant R_0 given that the lockdown merely functions to reduce R_0 to a smaller but constant value of Rt. For values of $R_0 \leq 2$ the dampening of the infection rate is so strong that herd immunity is not reached during the first year of the infection (blue orbit, Figure 7b). Once the measures of control are relaxed in the 13th month of the infection, a second wave of infections occurs immediately (yellow line, Figure 8d, blue orbit, Figure 7b).

For a mid-summer onset, seasonality combined with non-pharmaceutical controls dampen the infection rate during the initial months of the outbreak, but when winter arrives and the transmission-reducing effect of seasonality disappears, a peak infection of amplitude similar to the case of lockdown without seasonality effects occurs for values of $R_0 \geq 2.6$; (Figure 8a and b). This is demonstrated best for the case of R_0 = 2.6 in Figure 7c (orange orbit), where R_t first increases as winter is reached, where after it decreases as the disease runs its course in spring, with a clear crossing of the orbits of constant R_0. For smaller values of R_0, herd immunity is not reached during the first year of infection, thus once control measures are weakened second waves of infection follow (blue and yellow orbits in Figure 7c; red lines in Figure 7c and d). These do not occur immediately, as was the case in the absence of seasonality. Rather, the infection rate remains damped by seasonality in the summer and autumn of the second year of the disease, and peak infection only occurs in the winter or spring of the second year. For low values of R_0, most of the population is still susceptible after the first year of the infection (blue orbit, Figure 7c), and consequently the second wave of infections can be severe (in the absence of control measures being re-applied in the second year of the infection (red line, Figure 8d).

Under weak seasonality (ε = 0.1) the seasonality orbits are almost indistinguishable from those of constant R0 for the case of no control measures being applied (Figure 9a). However, for the realistic case of warm-cold seasonality as described by daily data for continental South Africa, where $\varepsilon \approx 0.2$, the seasonality orbits for high values of R_0 cross those of constant R0 (Figure 9b), consistent with the case

of ε = 0.2 (Figure 7a). Under stronger seasonality the SI-orbits display the same qualitative characteristics (Figure 9c). In the presence of lockdowns, despite more time effectively being allowed for seasonality to have an effect, its role remains limited when ε = 0.1 (Figure 9d). However, for continental South Africa ($\varepsilon \approx 0.2$) and stronger seasonal forcing in the presence of lockdown (Figure 9e and f), second waves of infections develop in the winter of the second year of the disease's propagation, with the formation mechanism similar as for Figure 7c.

4. Discussion

By late July 2020, eight months into the Covid-19 outbreak, it remains unclear whether transmission of SARS-CoV-2 is impacted by seasonal climate effects (e.g. O'Reilly et al., 2020). We modelled the outbreak of a highly infectious disease ($R0 \geq 2$), for the idealized cases of the initial infections occurring in mid-winter (when seasonality-influenced transmission rates are assumed to be highest) and mid-summer (trough in seasonality forcing) for a range of amplitudes of seasonality. Strong seasonal forcing may be expected to be found in the mid-latitudes, in regions that exhibit pronounced cold-warm (and thus generally also dry-moist) cycles, noting the current hypothesis that Covid-19 infection rates are optimal under cold and dry conditions. In such climates, the tell-tale signature of seasonality is the crossing of the SI-orbits of constant R0 by the seasonality orbits on an SI-diagram.

In the case of mid-winter onset, without control measures, the detectability of even strong seasonality ($\varepsilon \geq 0.2$) is limited for $R_0 > 2$ until about 50% of the population has been infected. For lower values of R0, the disease persist in the population for long enough for seasonality to be more clearly revealed. Control measures, which for now are non-pharmaceutical since no vaccine is as yet available reduce the infection rate, thereby slowing the progression of the disease. If a consistent level of control is applied for many months, the presence of seasonality can be clearly detected in the SI orbits. However, stringent lockdown measures prevent the development of herd immunity so that more than 70% of the population remain susceptible in the summer following the initial onset of the disease. Should control measures be relaxed in summer due to either a false sense of security that the disease has been contained, or under socio-economic pressure, severe seasonality-induced second waves can develop from autumn to spring of the following year. It may be noted that in this respect, current serological testing for SARS-Cov-2 specific antibodies in several countries, mostly in the Northern Hemisphere where Covid-19 had a winter onset, is suggesting that significantly less than 20% of the population had been infected by Covid-19 by time of the onset of the boreal summer of 2020 (e.g. Pollán et al., 2020).

When the disease onset occurs in mid-summer, the evolution of the disease is markedly different. Despite the dampening effects of climate, the disease still moves through the population for values of $R_0 > 2$ and herd immunity is reached before winter arrives. The seasonality-affected orbits cross the orbits of constant R_0 by the time that about half of the population has been infected. For lower values of R0 the disease is still propagating through the population by the time winter arrives and it reaches its full transmission probability, thus peak infection is similar to that in the absence of seasonality effects, with the seasonal orbits tangential to those of constant R_0. For very high values of R0 ($R_0 \geq 2.6$) stringent

control measures merely function to slow down the propagation of the disease. Considering seasonality, once winter arrives, the disease reaches its full transmission potential and peak infection is similar to that for the case of no seasonal effects. For lower values of R_0, the effect of lockdown is so substantial that herd immunity is not achieved in the first year of outbreak, and in the presence of seasonality second waves of high peak infection occur in the second year when winter sets in after control measures have been relaxed. Given the timing of the Covid-19 outbreak, this risk applies to Southern Hemisphere mid-latitude countries, including Australia and New Zealand, where efficient non-pharmaceutical control measures will apparently prevent herd immunity from being reached in 2020.

The tell-tale signature of seasonality is that the seasonal orbits cross those of a constant R0. The identification of this feature in real-world data, if it exists, will be confounded by inadequacies and differences in how infection rates are reported between countries. A further complicating factor is the temporally-varying application of non-pharmaceutical control measures. Nonetheless, we are of the view that this proposed test for seasonality can be successfully applied to operational data for a subset of countries, regions or cities, where bias-corrected testing programmes have been in place for several months and where periods of several months of consistent, known non- pharmaceutical control measures have been applied. It takes several months for the seasonality affected SI-orbits to cross the R0 orbits, under the realistic levels of the seasonality effect we explore here; and about half of the population needs to become infected for the seasonality feature to clearly develop. Given the limitations of operational Covid-19 statistics, the less than full annual cycle for which Covid-19 has been spreading on the planet and the fact that in most countries only a relatively small portion of the population has to date been infected, it is not surprising that no consensus has so far been reached in terms of seasonality impacts on Covid-19. The signal is obscured by both the noise of inconsistent data reporting, but also by the fundamental properties of the disease.

The following list of tests is proposed to objectively search for signatures of seasonality in operational Covid-19 (or any highly infectious disease) data:

1) Crossing of the SI-orbits of constant R0 by the seasonality

2) Differential rate at which the disease spreads for the case of mid-winter onset compared to mid-summer onset (mid-winter spread should be comparatively faster under similar conditions of non-pharmaceutical control).

3) Within a given country with summer onset of the disease, and under constant non- pharmaceutical control measures, an increase in Rt should be detected as winterapproaches; and for winter onset, a decrease as summer

4) The amplitude of peak infection (I/N) should be smaller for mid-summer onset compared to mid-winter onset, for cases where peak infection is reached ahead of winter (in the case of mid-summer onset).

5) The development of second waves of infection in the autumn through to spring of the second year of outbreak, in the absence of effective pharmaceutical or non- pharmaceutical

At the time of writing this paper (July 2020) Covid-19 is spreading rapidly in South Africa and many other Southern Hemisphere countries. Evidence of a clear influence of seasonality in this spread may still influence government decisions regarding the stringency and duration of lockdown measures. Under the assumptions made in this investigation, it is likely that Covid-19 will run its course in South Africa in the winter and spring of 2020, with herd immunity reached during 2020. Several South American countries seem to be on the same trajectory. The main application of clearer knowledge of Covid-19 seasonality is preparation for, or prevention of, second waves of infection. This is a clear risk for Northern Hemisphere countries in autumn to winter of 2020/21 and spring of 2021, and for Southern Hemisphere countries (in particular Australia and New Zeeland where non-pharmaceutical control has apparently contained the disease) in the winter and spring 2021. The successful development and widespread deployment of a vaccine would significantly reduce this risk. Conversely, if a vaccine is not generally available and those infected in 2020 do not obtain immunity, or lose that immunity within 12 months, the risks for second waves of infection in late 2021 will be large.

Clarity on the role of seasonality in Covid-19 outbreaks may be obtained within next few months by considering multiple lines of evidence. Careful comparison between the rate of spread and amplitude of peak infection in Northern Hemisphere vs Southern Hemisphere countries, as well as aseasonal tropical and high-latitude countries, may provide important clues. So may changes in climate in one location due to seasonal progression, on the condition that bias-corrected case data is also available. Examples where measures of lock-down or social distancing have not changed substantially during the course of the disease are especially useful, as is the comparison of locations with different climates but similar levels of non-pharmacological interventions. Problems with the different protocols for reporting cases, and different levels of testing, may be reduced by using death-rate anomalies as a proxy for Covid-19 mortality rates. An anomaly is the difference between the recorded number of deaths, which is usually relatively accurate across jurisdictions, and the seasonally-variable expected rate of deaths from all causes, based on long- term records. The anomaly can be inferred to be as a result of the direct and indirect effects of Covid-19. The corresponding infection rate can be estimated from the infection fatality rate, which is currently estimated to be 0.68% (0.53-0.82%) (Meyerowitz-Katz and Merone). As far as can be supported by reporting, sub-national data is far more useful than nationally-aggregated data, in large and climatically heterogeneous countries. The application of inverse modelling (e.g. Anastassopoulou et al.) is a rigorous evidence-driven approach to reconstructing the SI-orbits for particular locations from data on deaths, reported cases and *post-facto* serological testing. Until the importance of seasonality in Covid-19 infection rates has been established, it remains prudent to design control measures as if high temperature and humidity will *not* significantly dampen the infection rate (O'Reilly et al., 2020). At the same time, it is important to design control measures to cater for the possibility of severe, seasonality–induced second waves of infection. It is important for the Covid-19 seasonality question be answered ahead of the potential occurrence of second waves.

Declarations

Competing interests

The authors declare no competing interests.

Correspondence and requests for materials should be addressed to F.E.

References

Anastassopoulou C., Russo L., Tsakris A. and Siettos C. (2020). Data-based analysis, modelling and forecasting of the COVID-19 outbreak. *PlosOne*. DOI: 10.1371/journal.pone.0230405.

Baker R.E., Yang W., Vecchi G.A., Metcalf C.J.E. and Grenfell B.T. (2020). Susceptible supply limits the role of climate in the early SARS-CoV-2 pandemic. Science, DOI: 10.1126/science.abc2535.

Bukhari Q. and Jameel Y. (2020). Will coronavirus pandemic diminish by summer? SSRN, DOI: 10.2139/ssrn.3556998.

Chen S. and Epureanu B. (2017). Regular biennial cycles in epidemics caused by parametric resonance. *J Theor Biol.* **415** 137–44. doi:http://dx.doi.org/10.1016/j.jtbi.2016.12.013. PubMed.

Dushoff J., Plotkin J.B., Levin, S.A., Earn D.J.D. (2004). Dynamical resonance can account for seasonality of influenza epidemics. *Proc Natl Acad Sci USA.* **101** 16915–6. doi: http://dx.doi.org/10.1073/pnas.0407293101. PubMed.

Engelbrecht F.A., Adegoke J., Bopape M-J., Naidoo M., Garland R., Thatcher M., McGregor J., Katzfey J., Werner M., Ichoku C. and Gatebe C. (2015). Projections of rapidly rising surface temperatures over Africa under low mitigation. *Env. Res. Letters.* 10 085004.

Engelbrecht F.A., Marean C.W., Cowling R., Engelbrecht C., Nkoana R., O'Neal D., Fisher E., Shook E., Franklin J., Neumann F.H., Scott L., Thatcher M., McGregor J.L., Van der Merwe J., Dedekind Z. and Difford M. (2019). Downscaling Last Glacial Maximum climate over southern Africa. *Quaternary Science Reviews* **226** 105879. https://doi.org/10.1016/j.quascirev.2019.105879.

Escobara L.E., Molina-Cruz A. and Barillas-Mury C. (2020). BCG vaccine protection from severe coronavirus disease 2019 (COVID-19). *PNAS* www.pnas.org/cgi/doi/10.1073/pnas.2008410117.

Ficetola G.F. and Rubolini D. (2020). Climate affects global patterns of COVID-19 early outbreak dynamics. medRxi. DOI: 2020.03.23.20040501.

Gaunt E.R., Hardie A., Claas E.C., Simmonds P. and Templeton K.E. (2010). Epidemiology and clinical presentations of the four human coronaviruses 229E, HKU1, NL63, and OC43 detected over 3 years using a novel multiplex real-time PCR method. *J Clin Microbiol* **48** 2940–7.

Hale T., Webster S., Petherick A., Phillips T. and Kira B. (2020). Oxford COVID-19 Government Response Tracker, Blavatnik School of Government. https://www.bsg.ox.ac.uk/research/research-projects/oxford-covid-19-government-response-tracker

Harris I.C. and Jones P.D. (2020). CRU TS4.03: Climatic Research Unit (CRU) Time-Series (TS) version 4.03 of high-resolution gridded data of month-by-month variation in climate (Jan. 1901- Dec. 2018). Centre for Environmental Data Analysis, 22 January 2020. doi:10.5285/10d3e3640f004c578403419aac167d82. http://dx.doi.org/10.5285.

Kudo E., Song E., Yockey L.J., Rakib T., Wong P.W., Homer R.J. and Iwasaki, A. (2019). Low ambient humidity impairs barrier function and innate resistance against influenza infection. *Proc Natl Acad Sci USA* **116** 10905-10910. doi:10.1073/pnas.1902840116.

Lai S., Ruktanonchai N.W., Zhou L., Prosper O., Luo W., Floyd J.R., Wesolowski A., Santillana M., Zhang C., Du X., Yu H. and Tatem A.J. (2020). Effect of non-pharmaceutical interventions to contain COVID-19 in China. *Nature*. https://doi.org/10.1038/s41586-020-2293-x.

Lofgren E., Fefferman N.H., Naumov Y.N., Gorski J. and Naumov E.N. (2007). Influenza seasonality: underlying causes and modeling theories. *Journal of virology* **81** 5429-5436.

Lowen A.C., Mubareka S., Steel J. and Palese P. (2007). Influenza virus transmission is depen- dent on relative humidity and temperature. PLoS Pathog 3:1470–1476.

Lowen A.C., Steel J., Mubareka S. and Palese P. (2008). High temp (30 °C) blocks aerosol but not contact transmission of influenza virus. J Virol 82:5650–5652.

Maier B.F. and Brockmann D (2020). Effective containment explains subexponential growth in recent confirmed COVID-19 cases in China. *Science* https://doi.org/10.1126/science.abb4557.

Merow C. and Urban M.C. (2020). Seasonality and uncertainty in COVID-19 growth rates. medRxiv. doi: 10.1101/2020.04.19.20071951.

Meyerowitz-Katz G. and Merone L. (2020). A systematic review and meta-analysis of published research data on COVID-19 infection-fatality rates. medRxiv. doi: https://doi.org/10.1101/2020.05.03.20089854.

Neher R.A., Dyrdak R., Druelle V., Hodcroft E.B. and Albert Ja. (2020). Potential impact of seasonal forcing on a SARS-CoV-2 pandemic. *Swiss Med Wkly* **50** w20224. doi:10.4414/smw.2020.20224.

Nickbakhsh S., Ho A., Marques D.F.P., McMenamin J., Gunson R.N. and Murcia P.R. (2020). Epidemiology of Seasonal Coronaviruses: Establishing the Context for the Emergence of Coronavirus Disease 2019. *The Journal of Infectious Diseases* **222** 17–25.

O'Reilly K.M., Auzenbergs M., Jafari Y., Liu Y., Flasche S. and Lowe R. (2020). Effective transmission across the globe: the role of climate in COVID-19 mitigation strategies. *The Lancet Planetary Health* **4**

e172. https://doi.org/10.1016/S2542-5196(20)30106-6.

Pei S., Kandula S. and Shaman J. (2020). Differential Effects of Intervention Timing on COVID- 19 Spread in the United States. medRxiv preprint. doi: https://doi.org/10.1101/2020.05.15.20103655

Petrova V.N. and Russell C.A. (2020). The evolution of seasonal influenza viruses. *Nat Rev Microbiol.* **16** 47–60. doi: http://dx.doi.org/10.1038/nrmicro. 2017.118. PubMed.

Pollán M., Pérez-Gómez B., Pastor-Barriuso R., Oteo J., Hernán M.A., Pérez-Olmeda M., Sanmartín J.L., Fernández-García A., Cruz I., de Larrea N.F., Molina M., Rodríguez-Cabrera F., Martín M., Merino-Amador P., Paniagua J.L., Muñoz-Montalvo J.F., Blanco F. and Yotti R. (2020). Prevalence of SARS-CoV-2 in Spain (ENE-COVID): a nationwide, population-based seroepidemiological study. *The Lancet.* https://doi.org/10.1016/S0140-6736(20)31483-5.

Qi H., Xiao S., Shi R., Ward M.P., Chen Y., Tu W., Su Q., Wang W., Wang X., Zhang Z. (2020). COVID-19 transmission in Mainland China is associated with temperature and humidity: A time- series analysis. *Science of the Total Environment* **728**. DOI: 10.1016/j.scitotenv.2020.138778.

Sagripanti J.L. and Lytle C.D. (2007). Inactivation of influenza virus by solar radiation. *Photochemistry and photobiology* **83** 1278-1282.

Sajadi M.M., Habibzadeh P., Vintzileous A., Shokouhi S., Miralles-Wilhelm F. and Amoroso A. (2020). Temperature, Humidity, and Latitude Analysis to Estimate Potential Spread and Seasonality of Coronavirus Disease 2019 (COVID-19). *JAMA Network Open*. **3** e2011834-.

Sette A. and Crotty S. (2020). Pre-existing immunity to SARS-CoV-2: the knowns and unknowns. Nature Reviews Immunology. https://doi.org/10.1038/s41577-020-0389-z.

Shaman J., Pitzer V.E., Viboud C., Grenfell B.T. and Lipsitch M. (2010). Absolute humidity and the seasonal onset of influenza in the continental United States. *PLOS Biol.* **8** e1000316. doi:10.1371/journal.pbio.1000316 Medline.

Shaw Stewart P.D. (2016). Seasonality and selective trends in viral acute respiratory tract Infections. *Medical Hypotheses* **86** 104–119.

Silal S., Pulliam J., Meyer-Rath G., Nichols B., Jamieson L., Kimmie Z. and Moultrie H. (2020). Estimating cases for COVID-19 in South Africa update: 19 May 2020.

Wang J., Tang K., Feng K., and Lv W. (2020). High temperature and high humidity reduce the transmission of COVID-19. arXiv: arXiv:2003.05003v3.

Zhang J., Litvinova M., Liang Y., Wang Y., Wang W., Zha S., Wu Q., Merler S., Viboud C., Vespignani A., Ajelli M. and Yu H. (2020a). Changes in contact patterns shape the dynamics of the COVID-19 outbreak in China. *Science*. https://doi.org/10.1126/science.abb8001.

Zhang J., Litvinova M., Wang W., Wang Y., Deng X., Chen X., Li M., Zheng W., Yi L., Chen X., Wu Q., Liang Y., Wang X., Yang J., Sun K., Longini I.M. Jr., Halloran M.E., Wu P., Cowling B.J., Merler S., Viboud C., Vespignani A., Ajelli M. and Yu H. (2020b). Evolving epidemiology and transmission dynamics of coronavirus disease 2019 outside Hubei province, China: A descriptive and modelling study. *Lancet Infect. Dis.* S1473-3099(20)30230-9. doi:10.1016/S1473- 3099(20)30230-9pmid:32247326.

Figures

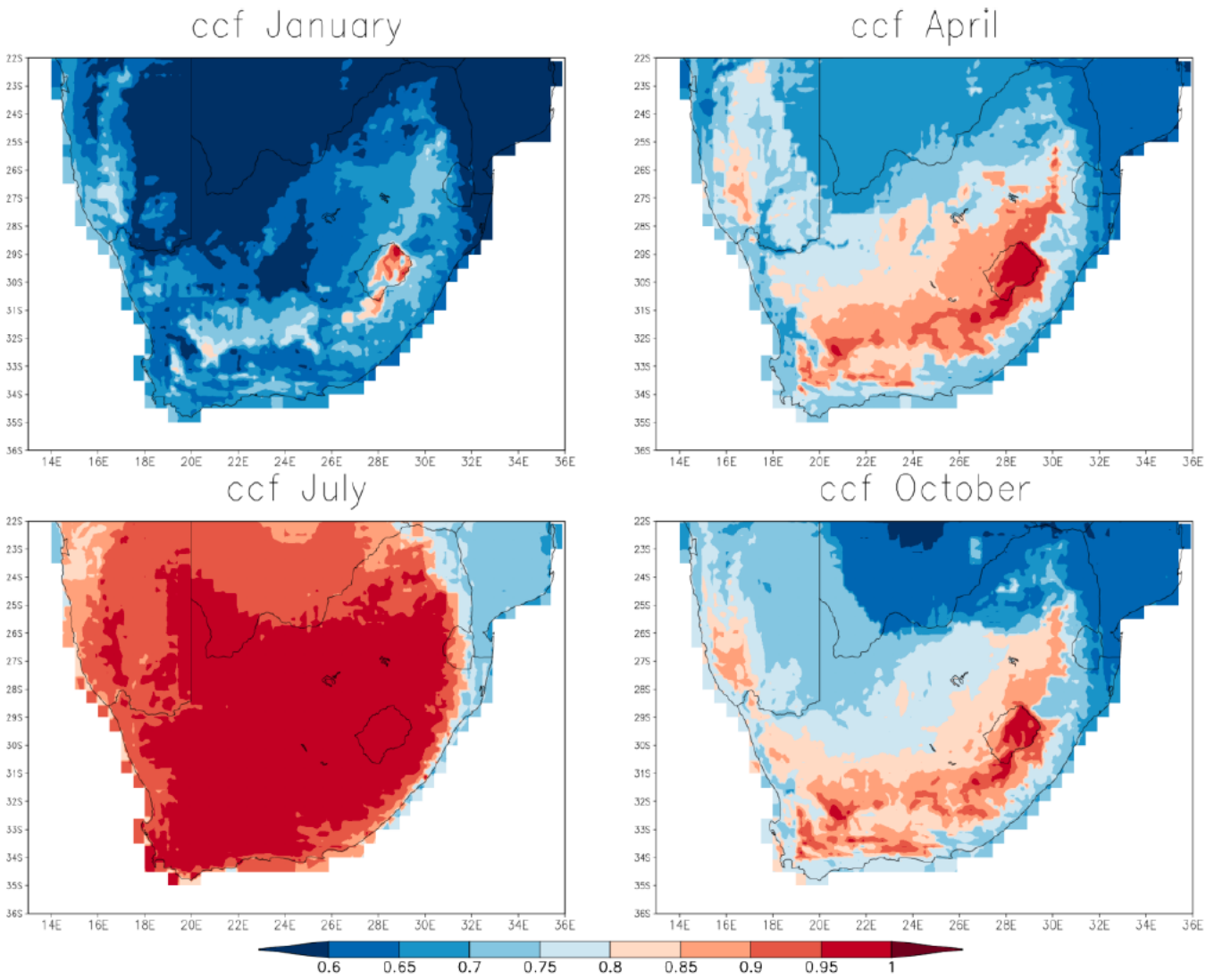

Figure 1

Example of application of the Climate correction factor (CCF), indicating how the Covid- 19 infection rate may be modified by temperature and humidity for the months January, April, July and October in South Africa.

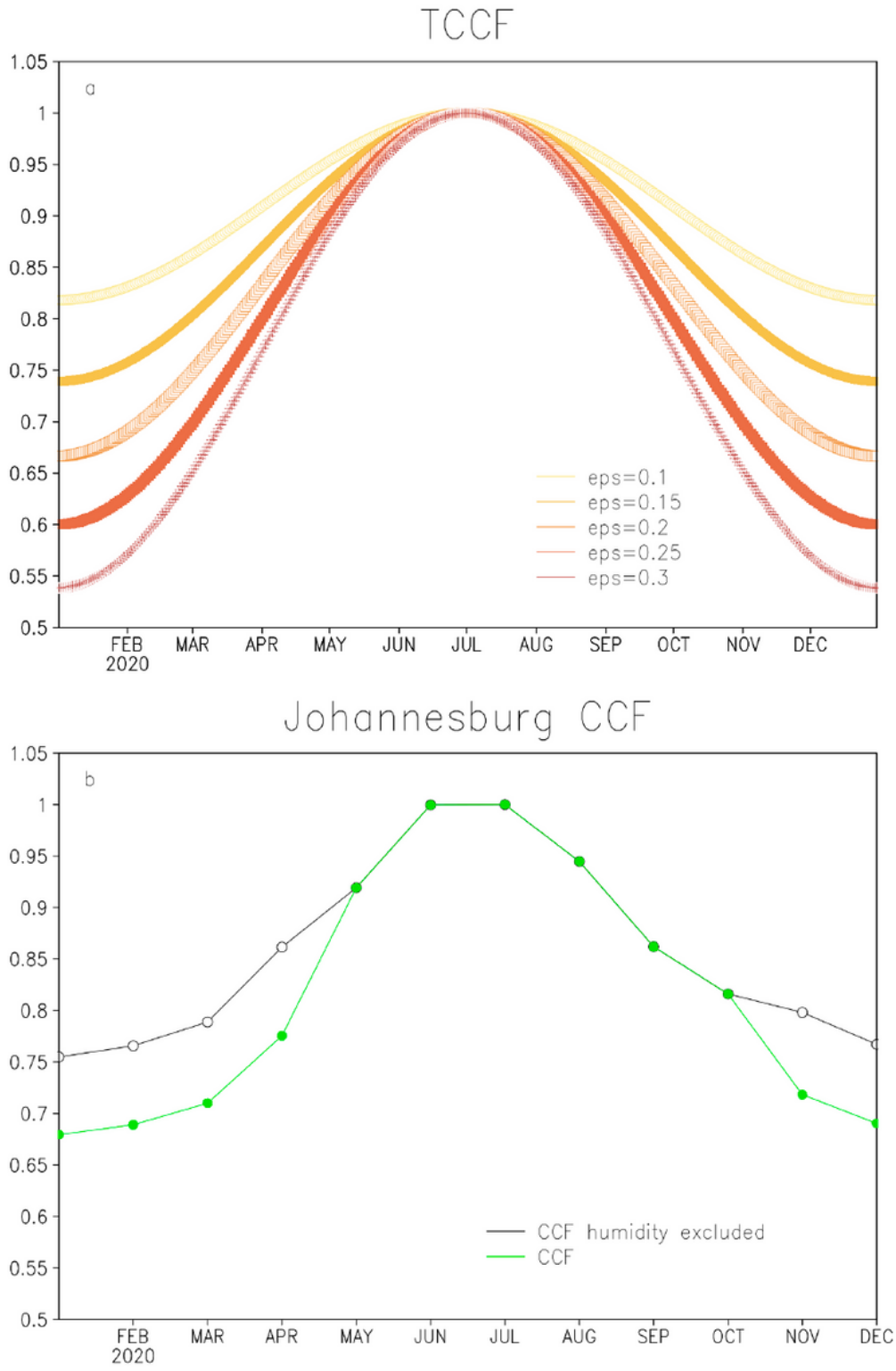

Figure 2

(a) TCCF for various values for 0.1 ≤ε≤ 0.3 (interval 0.05). (b) Observed seasonal cycle of the CCF in Johannesburg in the continental interior of South Afirca, showing temperature effects only (black lines) and both temperature and humidity effects (green lines) under (2).

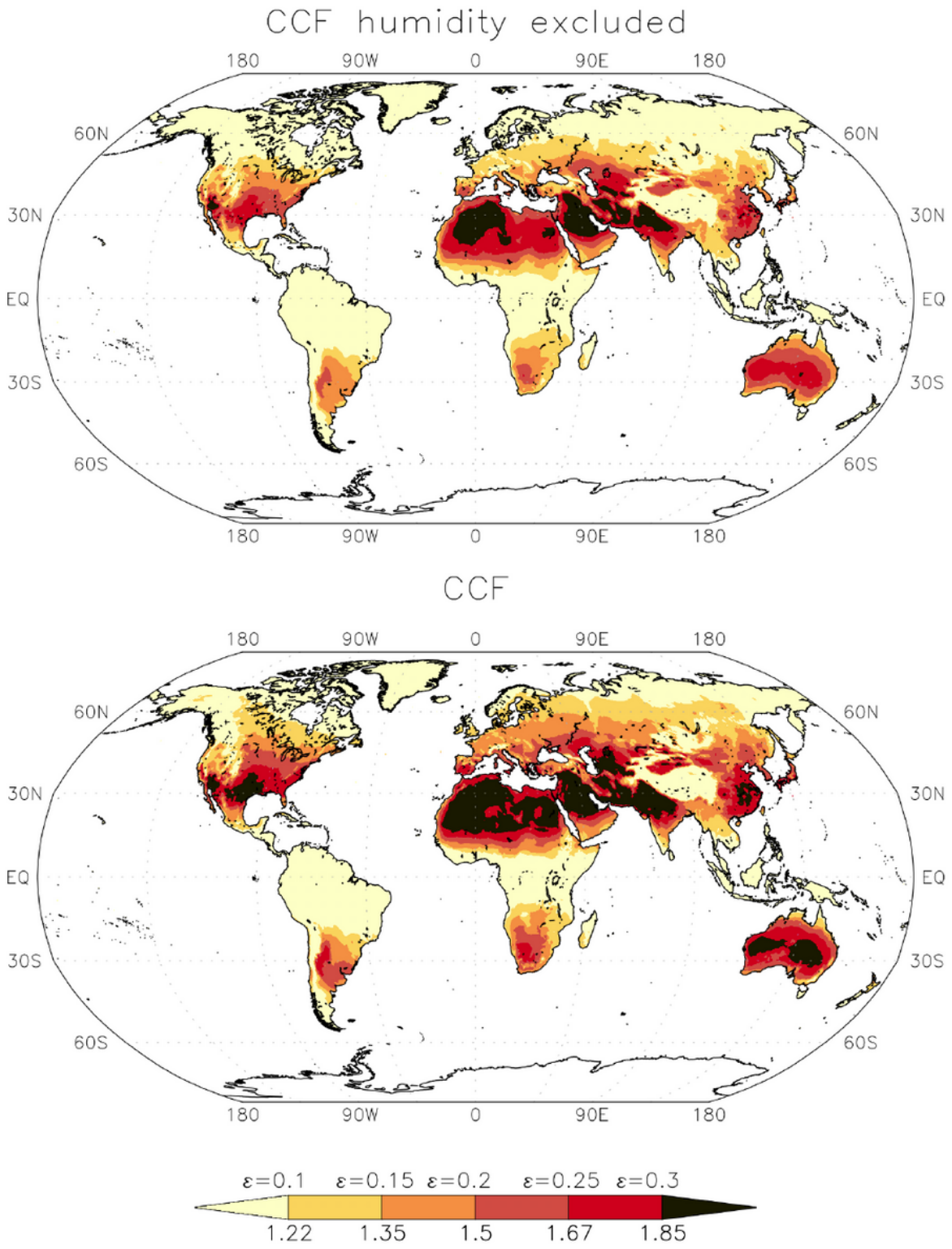

Figure 3

CCF seasonality amplitude with humidity effects excluded (top) and CCF amplitude (bottom) calculated over the period 2009-2018 using CRU TS4.03 data using (2), and shown in intervals corresponding to the seasonal amplitudes of ε = 0.1, 0.15, 0.2. 0.25, 0.3. Note: The designations employed and the presentation of the material on this map do not imply the expression of any opinion whatsoever on the part of Research Square concerning the legal status of any country, territory, city or area or of its

authorities, or concerning the delimitation of its frontiers or boundaries. This map has been provided by the authors.

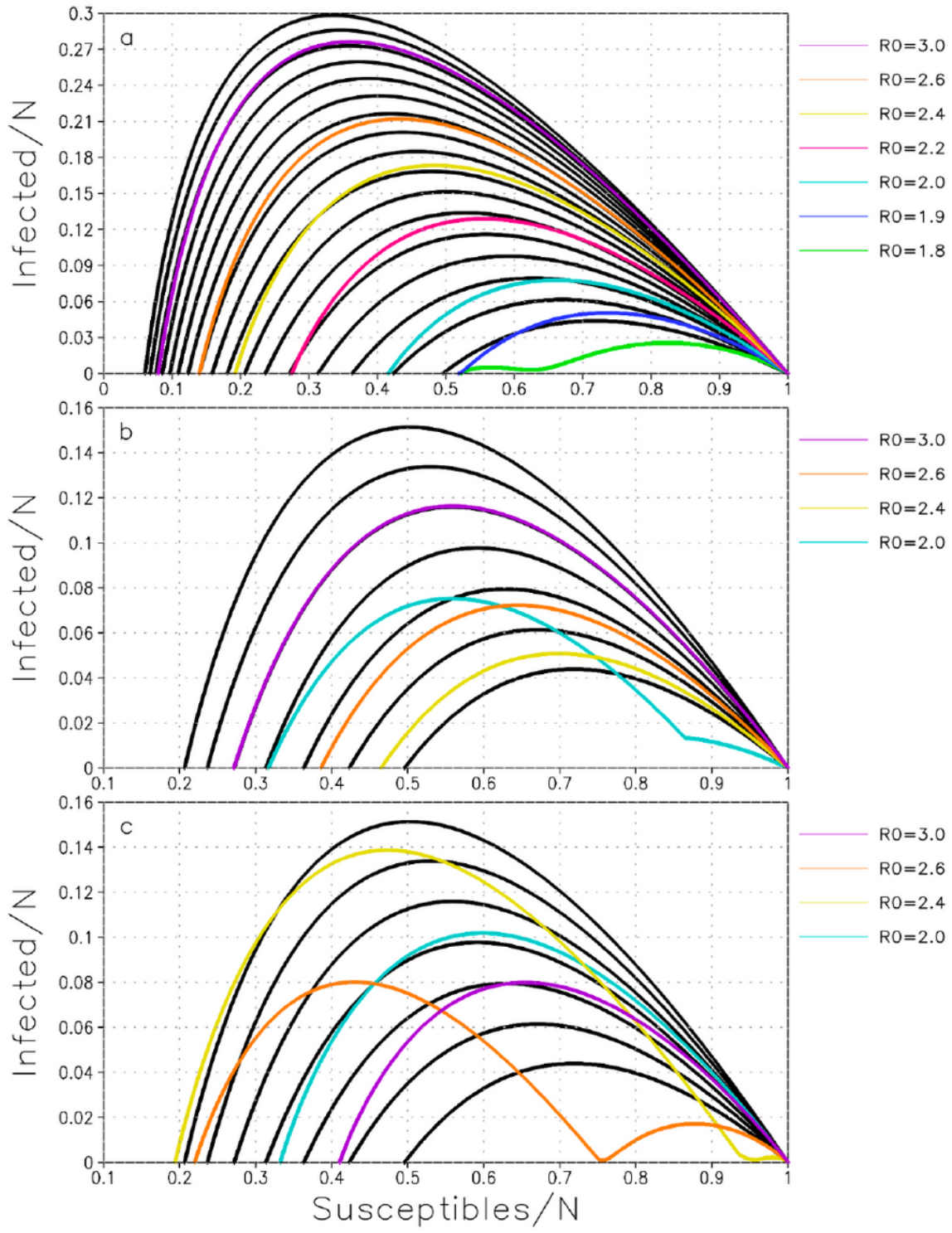

Figure 4

Susceptible-Infected (SI) orbits for various scenarios of non-pharmaceutical control measures and seasonality of ε = 0.2, for the case of mid-winter onset of an infectious disease. The orbits in black represent the scenario of no control with range and R0 interval [1.4, 3; 0.1] in a) and [1.4, 2; 0.1] in b) and

c). Note the different range of I/N in a) compared to b) and c). The colored lines orbits represent a) effects of seasonality for the scenario of no control; b) effects of a lockdown followed by social distancing and c) effects of lockdown followed by social distancing in combination with seasonality.

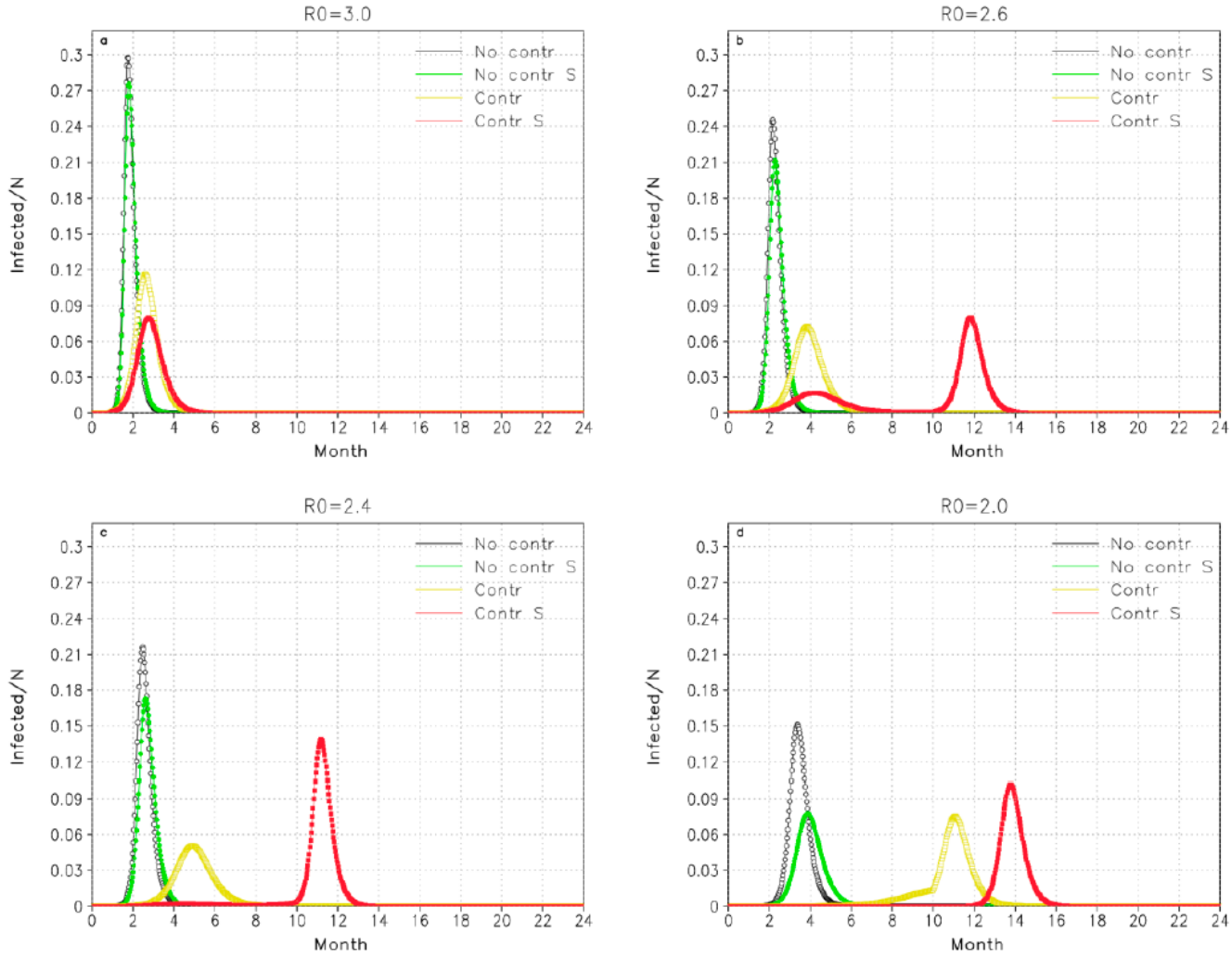

Figure 5

Evolution of I/N for an infectious disease for different values of R0 and where onset occurs in mid-winter. The black lines represents the scenario of no control measures and no seasonality, the green lines represent no control measures but with seasonality effects included, the yellow lines represent non-pharmaceutical control measures (see the text for details) and the red lines indicate the effects of seasonality in combination with non-pharmaceutical control. Seasonality is for ε = 0.2.

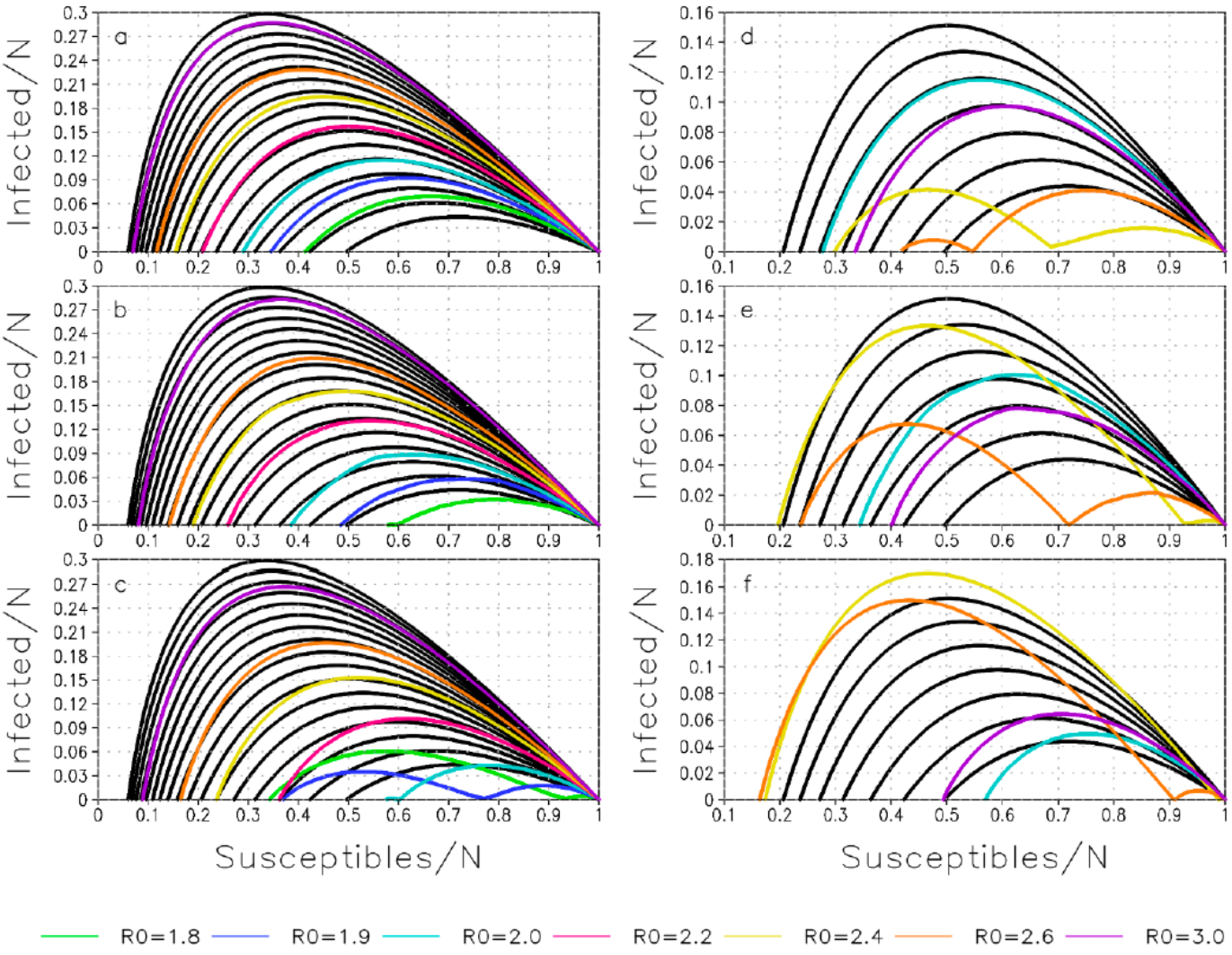

Figure 6

Susceptible-Infected (SI) orbits for mid-winter outbreak under different strengths of seasonality for scenarios of no control measures (left) and non-pharmaceutical control measures (right). In a) and d) ε = 0.1; b) and e) use realistic seasonal forcing (CCF based on function 2) from a continental climate with warm-cold seasonality in central South Africa and in c) and f) for ε = 0.3. The orbits in black represent the scenario of no control and no seasonality with range and interval of R0 of [1.4, 3; 0.1] in a) to c) and [1.4, 2; 0.1] in d) to f). Note the different range of I/N in the different panels. The colored lines orbits represent effects from seasonality in a) to c) and the combined effects of seasonality and non-pharmaceutical control in d) to f).

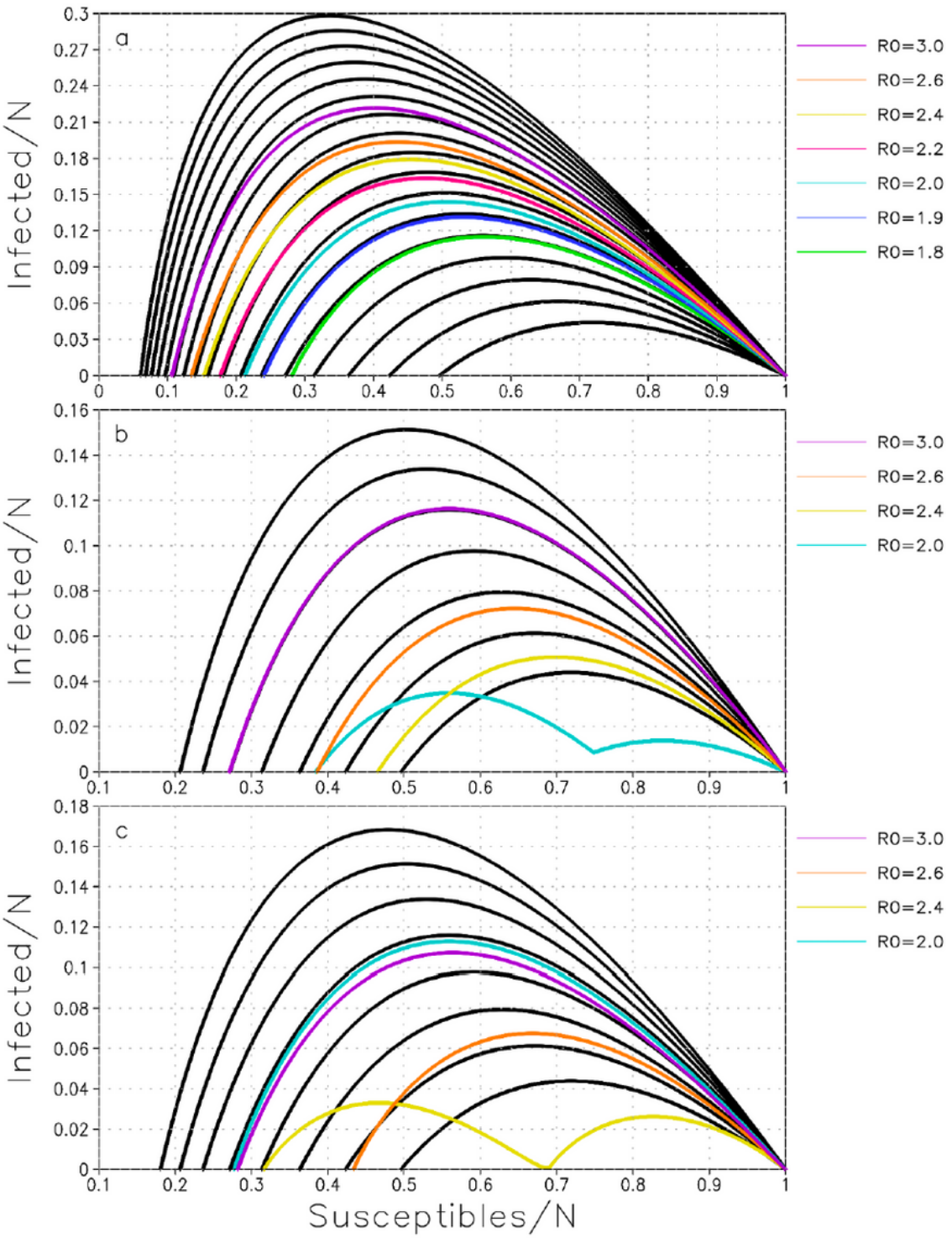

Figure 7

Susceptible-Infected (SI) orbits for various scenarios of non-pharmaceutical control measures and seasonality of ε = 0.2, for the case of mid-summer onset of an infectious disease. The orbits in black represent the scenario of no control with range and R0 interval [1.4, 3; 0.1] in a) and [1.4, 2; 0.1] in b) and c). Note the different range of I/N in a) compared to b) and c). The colored lines orbits represent a)

effects of seasonality for the scenario of no control; b) effects of a lockdown followed by social distancing and c) effects of lockdown followed by social distancing in combination with seasonality.

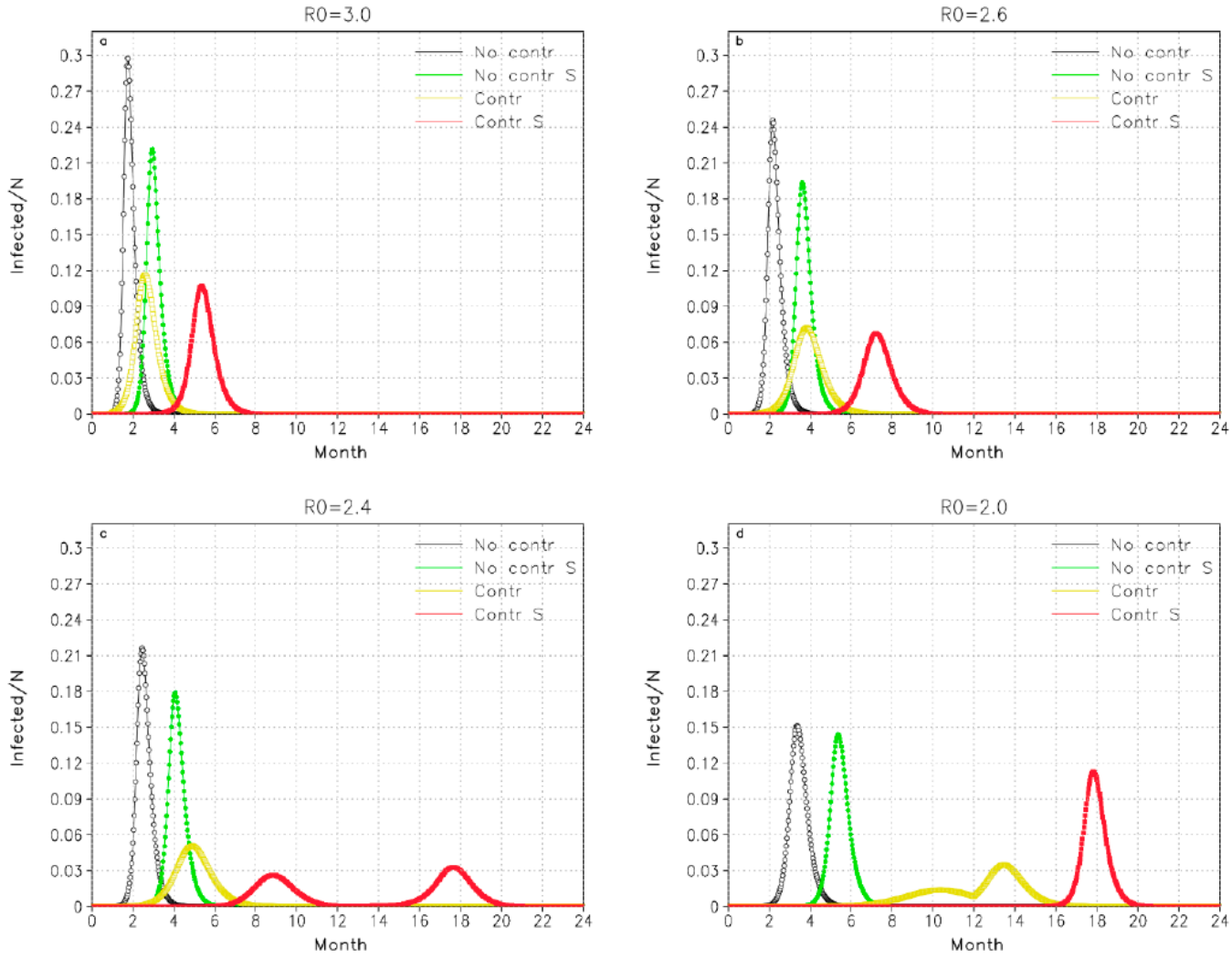

Figure 8

Evolution of I/N for an infectious disease for different values of R0 and where onset occurs in mid-summer. The black lines represents the scenario of no control measures and no seasonality, the green lines represent no control measures but with seasonality effects included, the yellow lines represent non-pharmaceutical control measures (see the text for details) and the red lines indicate the effects of seasonality in combination with non-pharmaceutical control. Seasonality is for ε=0.2.

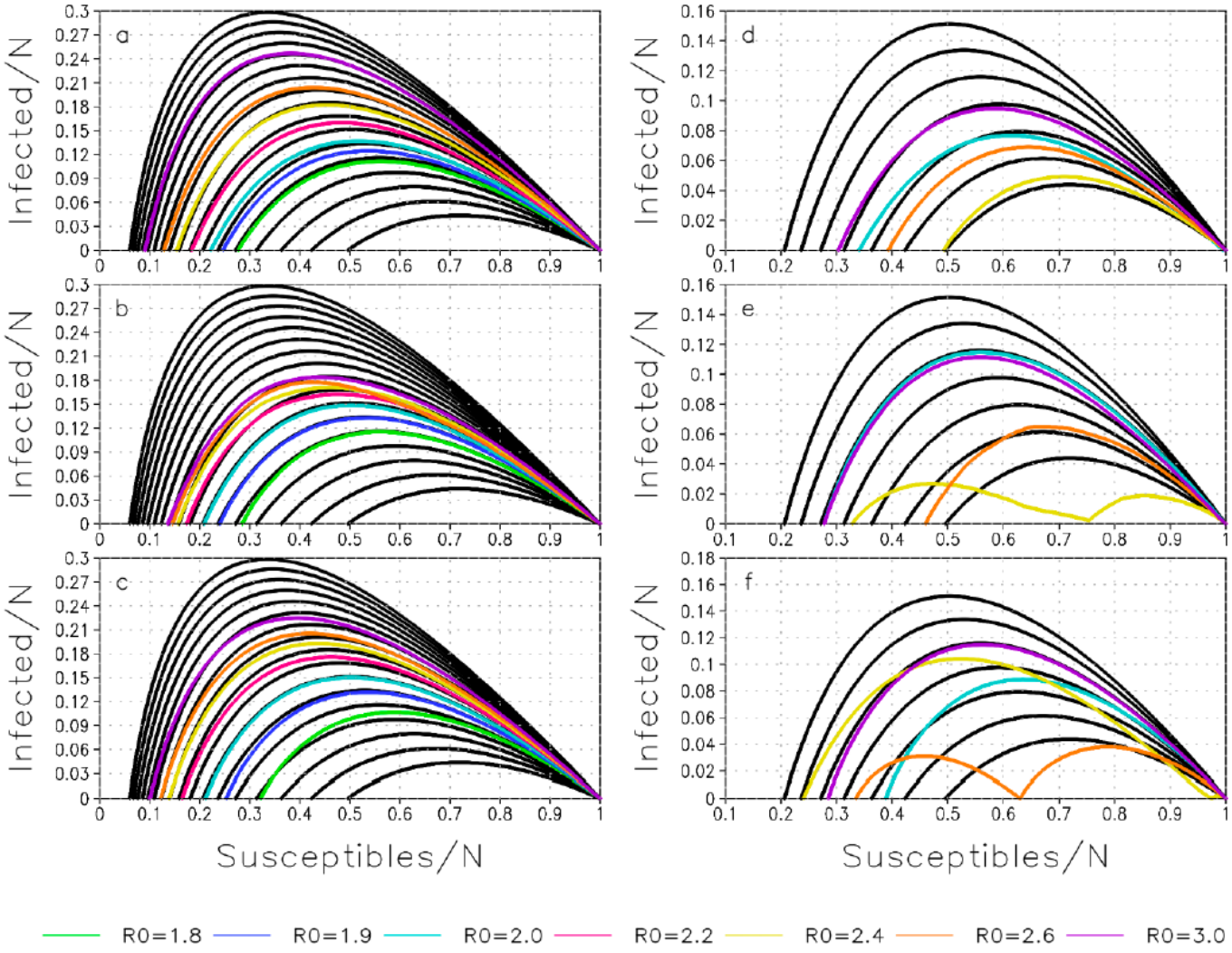

Figure 9

Susceptible-Infected (SI) orbits for mid-summer outbreak under different strengths of seasonality for scenarios of no control measures (left) and non-pharmaceutical control measures (right). In a) and d) ε = 0.1; b) and e) use realistic seasonal forcing (CCF based on function 2) from a continental climate with warm-cold seasonality in central South Africa and in c) and f) for ε = 0.3. The orbits in black represent the scenario of no control and no seasonality with range and interval of R0 of [1.4, 3; 0.1] in a) to c) and [1.4, 2; 0.1] in d) to f). Note the different range of I/N in the different panels. The colored lines orbits represent effects from seasonality in a) to c) and the combined effects of seasonality and non-pharmaceutical control in d) to f).